

Research Paper

Computer Modeling of Drug Delivery to the Posterior Eye: Effect of Active Transport and Loss to Choroidal Blood Flow

Ram K. Balachandran¹ and Victor H. Barocas^{2,3}

Received February 20, 2008; accepted July 17, 2008; published online August 5, 2008

Purpose. The direct penetration route following transscleral drug administration presents several barrier and clearance mechanisms—including loss to choroidal blood flow, active transport by the retinal pigment epithelium (RPE), and loss to the conjunctival lymphatics and episcleral blood vessels. The objective of this research was to quantify the role of choroidal and episcleral losses.

Materials and Methods. A finite element model was created for drug distribution in the posterior human eye. The volumetric choroidal loss constant, active transport component and mass transfer from the scleral surface were unknown parameters in the model. The model was used to simulate drug distribution from a systemic source, and the results were compared to existing experimental results to obtain values for the parameters.

Results. The volumetric choroidal loss constant, mass transfer coefficient from the scleral surface and active transport component were evaluated to be $(2.0 \pm 0.6) \times 10^{-5} \text{ s}^{-1}$, $(2.0 \pm 0.35) \times 10^{-5} \text{ cm/s}$ and $8.54 \times 10^{-6} \text{ cm/s}$ respectively.

Conclusion. Loss to the choroidal circulation was small compared to loss from the scleral surface. Active transport was predicted to induce periscleral movement of the drug, resulting in more rapid distribution and elevated drug concentrations in the choroid and sclera.

KEY WORDS: blood–vitreous barrier; fluorescein; fluorescein glucuronide; retinal pigment epithelium.

INTRODUCTION

Posterior segment eye diseases cause vision impairment and blindness in millions of people. A number of these diseases, including age-related macular degeneration, glaucoma, and diabetic retinopathy can cause irreversible blindness and are currently treated with the help of drugs (1). Delivering drugs to the posterior eye is a challenge because of the presence of various physiological and anatomical barriers. Systemic delivery is not feasible because of the small size of the eye and resulting small blood supply. Also, the blood–vitreous barrier presents a hindrance to drug penetration from the blood to the vitreous (2). The inefficiency of systemic delivery requires very large doses, placing non-targeted tissues at risk. Topical delivery (eye drops) is also ineffective in producing therapeutic concentrations in the posterior eye because of a series of impediments: lacrimation and tear dilution, the corneal epithelium, absorption by the conjunctiva, and rapid elimination by the aqueous humor flow. It has been shown that less than 3% of aqueous instilled

dose reaches the aqueous humor (3). Intravitreal delivery of drugs through implants and injections has been associated with serious side effects like endophthalmitis, hemorrhage, and retinal detachment (4). Also, since repeated administrations are needed to maintain effective drug levels, the risk of injury to the eye is high, and patient tolerance is poor. The shortcomings of existing delivery methods necessitate a novel delivery concept. The sclera has been shown to be highly permeable to a large number of macromolecules (5–10), creating interest in the transscleral route to deliver drugs to the posterior eye. The method is less invasive than intravitreal delivery and also provides the option of localized sustained delivery.

Many drugs used to treat vitreoretinal diseases have a narrow concentration window within which they are effective (11). Higher concentrations can be toxic, and lower concentrations can be insufficient to treat the disease. Hence, for a transscleral delivery system to be effective, it is critical to be able to predict drug concentrations within the eye following administration. In response, there have been several computational models developed to simulate the distribution and elimination of drugs from the posterior eye (see Table I). In developing such a model, one must address three important mechanisms for drug transport: loss to the choroidal circulation, active transport by the retinal pigment epithelium (RPE), and loss to the conjunctival lymphatics and episcleral veins. Fig. 1 shows the different layers of the posterior eye and the location of the transport mechanisms.

¹Department of Mechanical Engineering, University of Minnesota, Minneapolis, Minnesota, USA.

²Department of Biomedical Engineering, University of Minnesota, 7-105 Nils Hasselmo Hall, 312 Church Street SE, Minneapolis, Minnesota 55455, USA.

³To whom correspondence should be addressed. (e-mail: baroc001@umn.edu)

Table I. Drug Transport Models in Posterior Eye

Reference	Geometry	Choroidal losses	Active transport
(40)	Sphere	Ignored	Ignored
(16)	Spherical shells	Ignored	Outward and inward permeability of BRB calculated
(60)	Cylinder	Ignored	Ignored
(61–63)	Physiological (Human/rabbit eye)	Ignored	Ignored
(17)	Physiological (Human/mouse eye)	Ignored	Coupled with loss from vitreous
(34)	Physiological (rabbit eye)	Suggested a method to include vascular clearance effects	Ignored
(35)	Physiological (rabbit eye)	Complete sink	Ignored
(41)	Physiological (rabbit eye)	Complete sink	Ignored

Choroidal blood flow is among the highest per unit volume in the body. A vast network of vessels, the choriocapillaris, delivers oxygen and nutrients to the eye, and it could serve as a sink for transclerally delivered drugs, preventing them from reaching the target. As seen in Table I, choroidal losses have been ignored in some cases, lumped with the episcleral clearance route in some, and treated as a perfect sink in others.

Active transport by the RPE has been demonstrated for water (12) and some test solutes (13–15). This active transport could be significant compared to passive diffusion and convection, but it has been largely ignored in previous models. Yoshida *et al.* (16) estimated the inward and outward permeability of the blood-retinal barrier and attributed a higher outward permeability to the existence of an active transport mechanism. Stay *et al.* (17) included active transport of aqueous humor in the clearance of the drug from the vitreous in their model of intravitreal drug delivery.

Losses to the conjunctival lymphatics and episcleral veins are of obvious importance for any drug outside the sclera. The work of Robinson *et al.* (18) suggests that this drainage route may have a profound effect on transscleral delivery. Most previous models have treated the episcleral space as a perfect sink.

The major challenge in modeling such phenomena is the difficulty in isolating and measuring their individual effects. For example, an MRI study on transscleral delivery in living *vs.* dead rabbits (18) found significant differences, but whether those differences were due to choroidal losses, active RPE transport, or other factors, is not clear. The objectives of this work were therefore to develop a computational model of transport in the posterior eye, to incorporate choroidal

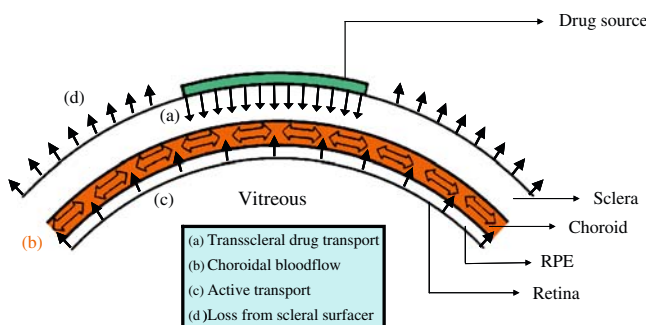
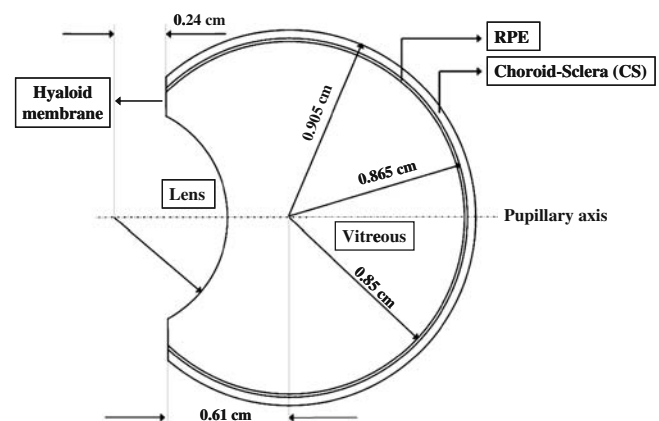
losses and active transport into that model, and to apply that model to published experimental studies and evaluate the model parameters associated with choroidal losses and active transport.

MATERIALS AND METHODS

Model Development and Conservation Equations

A three-dimensional model was developed based on the posterior segment of the human eye (17,19) (Fig. 2). The domain is defined by six main tissues: the retina, the choroid, the sclera, the vitreous, the lens, and the hyaloid membrane, which combines with the lens to form a partition between the anterior eye and the posterior eye. For the purpose of modeling, we have lumped the choroid and sclera together into one entity, the CS layer. The lumped tissue forms the boundary for the vitreous on the posterior surface, and the lens and hyaloid membrane bound the vitreous on the anterior surface. Only half of the posterior eye was modeled due to symmetry about a plane passing through the transscleral drug source (if present) and the pupillary axis.

Both convection and diffusion play an important role in determining the distribution and the eventual elimination of the drug from the posterior eye. Convection is due to the steady permeation of the aqueous humor through the vitreous, and diffusion is driven by the concentration gradient. We treat the vitreous as stagnant and incompressible

**Fig. 1.** Transport routes and barriers for transscleral drug delivery.**Fig. 2.** Schematic of the geometry of the posterior human eye model showing the domains and the boundaries along with their dimensions.

under normal conditions (20,21). The Darcy flow equation, which describes flow through a static, incompressible porous medium, can therefore be applied

$$v = -\frac{K}{\mu}\nabla P \quad (1)$$

where K is the permeability of the vitreous and μ is the viscosity of the permeating aqueous. The term K/μ is collectively referred to as the hydraulic conductivity. Equation 1 is also applied to the retina and the choroid/sclera with the hydraulic conductivity modified appropriately. The scleral hydraulic conductivity, scaled for the thickness, was used for the conductivity of the CS layer because the scleral resistance to transport is much greater than the resistance of the choroid (22). Since the aqueous humor is incompressible,

$$\nabla \cdot v = 0; \Rightarrow \frac{K}{\mu}\nabla^2 P = 0 \quad (2)$$

To model the drug distribution in the vitreous, we applied the mass balance equation for the drug:

$$\frac{\partial c}{\partial t} + v \cdot \nabla c - D_v \nabla^2 c + q = 0 \quad (3)$$

where c represents the concentration of the drug, D_v is the diffusion coefficient of the drug in the vitreous, v is the velocity of aqueous permeation from Eq. 1, and q is the generation/consumption rate of the drug. We assumed that the drug is not metabolized or otherwise degraded within the vitreous, so the generation/consumption term q was set to zero within the vitreous. An intravitreal controlled-release source would be modeled by a negative q (17).

The blood-vitreous barrier is comprised of the retinal pigment epithelium and the retinal and choroidal capillaries. The barrier has been shown to be asymmetric with respect to the transport of fluorescein (23–27). The outward permeability (vitreous to blood) of fluorescein is roughly 100 times higher than the inward permeability (28). This asymmetry has been attributed to active pumping by the RPE, which is known to pump water from the retinal space into the choroidal circulation (29). The mass transport equation was modified for the retina as:

$$\frac{\partial c}{\partial t} + (v + k_{\text{act}}) \cdot \nabla c - D_{\text{ret}} \nabla^2 c = 0 \quad (4)$$

where D_{ret} is the diffusivity of the drug through the retinal layer. The unidirectional pumping mechanism is modeled with the help of an added convective velocity, k_{act} , a vector pointing in the radially outward direction, of magnitude k_{act} .

The drug mass balance equation was modified for the CS to account for the exchange of the drug between the tissue and the choroidal circulation as a source/sink term:

$$\frac{\partial c}{\partial t} + v \cdot \nabla c - D_{\text{cs}} \nabla^2 c - \gamma(c_{\text{bl}} - c) = 0 \quad (5)$$

where c_{bl} represents the concentration of the drug in the blood, and D_{cs} represents the diffusivity of the drug in the CS tissue, which is set equal to the diffusivity of the drug in the sclera alone. The rationale behind this assumption is similar

to that for the hydraulic permeability of the CS layer. The source and the loss terms are modeled as a linear function of concentration with γ representing the rate constant for volumetric drug transport across the blood vessels in the choroid. The term $\gamma(c_{\text{bl}} - c)$ represents a systemic source term when $c_{\text{bl}} > c$ and a sink term when $c_{\text{bl}} < c$.

After systemic administration, drugs enter the posterior eye tissues mainly through the blood vessels in the choroid. A comparatively small amount could also diffuse out of the blood into the anterior tissues, overcoming the relatively weak blood-aqueous barrier, and later diffuse to the posterior eye. However, the small amount of drug that enters the anterior segment is largely eliminated by the anterior flow of the aqueous humor. Hence, a systemic drug source is assumed to be evenly distributed in the choroid, and any contribution from the anterior segment tissues was neglected (30).

Boundary Conditions

Since the model equations are second-order partial differential equations, conditions must be specified at each boundary for both pressure and concentration. The lens is avascular and impermeable to water, so we specify that there be no permeation of aqueous humor through the lens.

$$n \cdot v = 0 \Rightarrow n \cdot \nabla P = 0 \quad (6)$$

where n is the outward unit surface normal at the lens surface. Similarly, the normal component of the concentration flux at the lens surface is also equated to zero as we assume that the drug (fluorescein is used as the model drug) does not penetrate the lens (31). Hence,

$$n \cdot (-D_v \nabla c + vc) = 0 \quad (7)$$

It should be noted though, that lipophilic drugs might partition favorably into the lens (32) and equation (7) would need to be modified accordingly.

The hyaloid membrane is the highly porous membrane that separates the vitreous from the anterior segment of the eye. Because of the relatively thin structure and high porosity of the membrane, it offers negligible resistance to flow, and hence we have assumed that the pressure at the hyaloid is equal to the pressure in the anterior segment, the intraocular pressure (IOP). In a normal, healthy individual, IOP is roughly 15 mmHg or 2,000 Pa. The pressure at the outer surface of the CS membrane is set to be equal to the episcleral venous pressure which is around 10 mmHg or 1,300 Pa (33). Thus the total pressure drop across the posterior segment of the eye is 5 mmHg, comparable to expected values (33).

Since the anterior segment was not included in the model, we have included a flux boundary condition, similar to the procedure used by Missel (34), to represent the loss of the drug to the anterior segment. Assuming that the aqueous humor in the posterior chamber is well mixed, the flux of the drug at the hyaloid surface was expressed as:

$$n \cdot (-D \nabla c + vc) = (f/A)c = k_{\text{hy}}c \quad (8)$$

where f is the turnover rate of aqueous humor [2.5 $\mu\text{l}/\text{min}$ (20)], A is the hyaloid membrane area (2.4 cm^2), and c is the

concentration at the hyaloid surface. The combined constant k_{hy} , which is equal to f/A , is used to represent the mass transfer coefficient at the hyaloid surface.

The loss of drug from the scleral surface is an important factor affecting drug transport in the posterior eye. Recently, Kim *et al.* (35,36) used MRI to follow the movement of gadolinium-diethylenetriaminopentaacetic acid (Gd-DTPA), a drug surrogate and a magnetic contrast agent, after placing an episcleral implant at the equator of the eye. They found that elimination into the conjunctival lymphatics and the episcleral veins from the scleral surface played an important role in reducing vitreous concentration levels. The boundary condition at the scleral surface was modeled as:

$$n \cdot (-D\nabla c + vc) = k_{sc}c \quad (9)$$

where k_{sc} represents the mass transfer coefficient at the scleral surface. The coefficient k_{sc} includes loss to the conjunctival lymphatics and episcleral veins, and any other possible elimination mechanisms.

Model Parameters

The model parameters are listed in Table II. The model has three unknown parameters, namely γ , k_{act} , and k_{sc} , which were evaluated in this work. The constants γ and k_{sc} were evaluated by comparing model results to existing experimental data, and k_{act} was evaluated based on the ratio of strength of unidirectional to bidirectional transport across the blood-vitreous barrier using equation (10). A detailed description of the procedure follows in the solution methodology section and the results section. The diffusivities listed in the table are those of sodium fluorescein, which was used as the model compound for the simulations. Fluorescein was used because of the numerous studies, both experimental and theoretical that has been done on the transport of the compound through the vitreous and sclera of animals.

Solution Methodology

The first step in the solution process was to solve for the pressure distribution. The pressure distribution in the poste-

rior eye was assumed to be unaffected by drug transport and hence time-independent. The pressure was solved using the finite element method. The method is described in greater detail at the end of the section. The velocity of aqueous permeation was calculated from the pressure values and was used in the mass balance equations for the drug to solve for the concentration. The final step in the process was to compare the transient concentration values with published experimental results to obtain estimates for the unknown parameters.

Palestine and Brubaker (26) studied the pharmacokinetics of fluorescein in the vitreous of normal individuals after intravenous and oral fluorescein administration. Free plasma fluorescein concentration in the blood and average vitreous fluorescein concentration were measured over an 8 h period. The forcing term for the model, c_{bl} , was set equal to the free plasma fluorescein concentration measured by Palestine and Brubaker, and the average vitreous concentrations were calculated from the simulations.

Several studies (16,28,37,38) have shown that fluorescein, after systemic administration rapidly metabolizes into a fluorescent metabolite, fluorescein monoglucuronide (FG) and that the strength of active transport of FG is lesser when compared to fluorescein. Since Palestine's experimental measurements did not distinguish between fluorescein and FG, we assume that the measured vitreous concentrations were a combination of fluorescein and FG and not fluorescein alone.

The relationship between the unidirectional and bidirectional components in the posterior tissues in our model was assumed to be

$$\frac{\left(\frac{L_{rpe}^2}{D_{rpe}} + \frac{L_{cs}^2}{D_{cs}} + \frac{1}{\gamma}\right)}{\frac{L_{rpe}}{k_{act}}} = Pe^* \Rightarrow k_{act} = \frac{Pe^* L_{rpe}}{\left(\frac{L_{rpe}^2}{D_{rpe}} + \frac{L_{cs}^2}{D_{cs}} + \frac{1}{\gamma}\right)} \quad (10)$$

where L_{cs} and L_{rpe} are the thicknesses of the CS and the RPE layers. Bidirectional transport (passive transport) includes diffusion in the RPE, diffusion in the choroid-sclera, and passive exchange of drug between the choroidal blood vessels and the tissue. Unidirectional transport includes the active transport by the RPE. Pe^* (strength of active to passive

Table II. Parameter Values Used for the Simulation

	Parameter	Value	Reference
Vitreous	$(K/\mu)_v$	$8.4 \times 10^{-7} \text{ cm}^2/\text{Pa}\cdot\text{s}$	Xu <i>et al.</i> (21)
	D_v	$6.0 \times 10^{-6} \text{ cm}^2/\text{s}$	Stay <i>et al.</i> (17)
Retina	$(K/\mu)_{ret}$	$2.36 \times 10^{-11} \text{ cm}^2/\text{Pa}\cdot\text{s}$	Tsuboi (12)
	D_{ret}	$3.9 \times 10^{-7} \text{ cm}^2/\text{s}$	Park <i>et al.</i> (41)
CS	$(K/\mu)_{cs}$	$1.5 \times 10^{-11} \text{ cm}^2/\text{Pa}\cdot\text{s}$	Fatt <i>et al.</i> (20)
	D_{cs}	$1.0 \times 10^{-6} \text{ cm}^2/\text{s}$	Missel (34)
Hyaloid (BC)	$P_{hyaloid}$	15 mmHg (2,000 Pa)	
Sclera (BC)	k_{hy}	$1.73 \times 10^{-5} \text{ cm/s}$	Missel (34)
	P_{sclera}	10 mmHg (1,333.33 Pa)	Blondeau <i>et al.</i> (33)
Barrier constants	k_{sc}	$2.03 \times 10^{-5} \text{ cm/s}$	Regressed to (26)
	γ	$1.98 \times 10^{-5} \text{ s}^{-1}$	Regressed to (26)
	k_{act} (fluorescein)	$3.1 \times 10^{-5} \text{ cm/s}$	Set so $Pe^*=109$ (28) (see "Results")
	k_{act} (fluorescein and FG)	$8.54 \times 10^{-6} \text{ cm/s}$	Set so $Pe^*=30$ (26) (see "Results")

k_{sc} , γ and k_{act} were calculated in the study.

transport) is modeled similar to that of Péclet number (Pe) in standard species balance equations by using the time scales for passive and active transport. The ratio of time scales were used instead of the ratio of permeabilities since, the length scales for bidirectional and unidirectional transport are not the same as active transport is assumed to be present only in the RPE. Pe^* is set to 30 for comparison with Palestine and Brubaker's data, a conservative value based on available data on the active transport of fluorescein and FG (see Table III). In Eq. 10, all of the parameters are known except for k_{act} and γ , so γ is treated as an independent quantity, with k_{act} defined by Eq. 10.

The Gauss–Newton iterative scheme was used to obtain the best fit between the simulated average vitreous concentrations and the experimental concentrations. The iterative scheme involves solving for the partial derivatives of the concentration with respect to the two independent parameters γ and k_{sc} . A brief discussion of the scheme is included in Appendix. The Galerkin finite element method (GFEM) was used to solve the partial differential equations for pressure and concentration, and a multi-module C code was written to do the same. The vitreous, RPE and the CS layers were divided into 40, 20 and 30 finite elements each along the radial direction (see Fig. 2). The sclera, retina and the lens faces were divided using 268 elements. Hence, a total of 24,120 elements were used to model the domain. Each element consisted of 27 nodes with each node having one degree of freedom. A total of 205,073 nodes were used in the model. Triquadratic basis functions were used to interpolate between the nodes for both pressure and concentration. GFEM method was used to discretize the spatial derivatives, and the implicit Euler scheme was used to integrate the resulting ordinary differential equations in the time domain. MUMPS (39) (Multi frontal massively parallel sparse direct solver) was used to solve the resulting algebraic equations. The problem was solved on an SGI-Altix using a single processor as the computational demand was not large. Typical run times were 15 CPU-hours.

RESULTS

Pressure and Aqueous Permeation Velocity

The pressure in the vitreous was found to be almost uniform, with the drop in value being less than 2 Pa. The vast difference in the hydraulic conductivity between the vitreous

Table III. Strength of Active to Passive Transport Values

Source	Species	Pe^*
Miyake (24)	Human	27
Zeimer <i>et al.</i> (27)	Human	30
Blair <i>et al.</i> (23)	Human	31
Oguro <i>et al.</i> (25)	Human	31
Cunha-vaz and Maurice (13)	Rabbit	37
Palestine and Brubaker (26)	Human	38
Engler <i>et al.</i> (28)	Human	109
Yoshida <i>et al.</i> (16)	Monkey	160

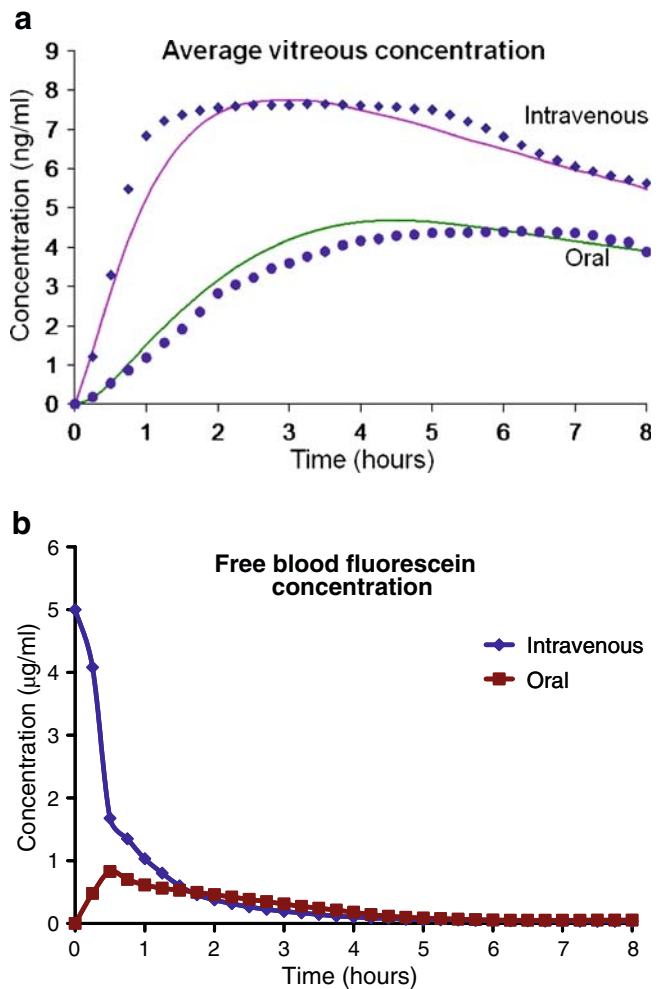


Fig. 3. **a** Best fit between experimental and simulated data. Dots represent the experimental data points and the continuous line represents the simulation results. **b** Free blood fluorescein concentration used for the simulation. The values were obtained from Palestine and Brubaker (26).

and the other posterior tissues results in almost the entire pressure drop being across the retina, choroid, and sclera.

Aqueous flow within the vitreous is relatively more important when compared to the retina and the CS membrane as convection within the vitreous might result in better drug delivery to the macula and the other central regions of the retina. The average velocity at the retinal surface calculated from the model was 2.9×10^{-7} cm/s, consistent with earlier analysis (17,34,35,40,41). The total aqueous outflow through the vitreous was $0.069 \mu\text{l}/\text{min}$, which is 2.8% of the total aqueous humor produced.

Comparison of Model Results with Available Experimental Data

Fig. 3a shows the best fit obtained between the simulated vitreous concentrations and experimentally determined concentrations published by Palestine and Brubaker. The free blood fluorescein concentration measured by the investigators, which was used as an input to the model, is shown in Fig. 3b. The 95% confidence ranges for the barrier and clearance

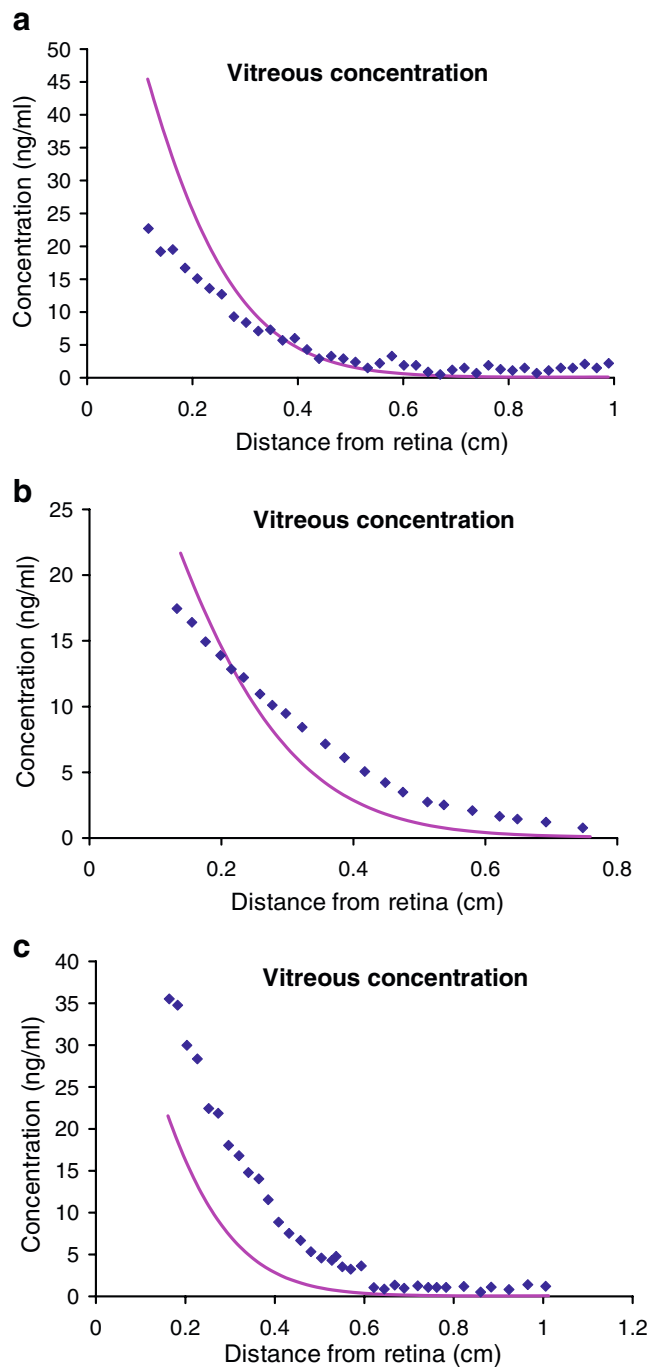


Fig. 4. Comparison of simulated and experimental vitreous concentration (fluorescein and FG). Dots represent the experimental data points and the continuous line represents the simulation results. **a** 63 min after systemic administration. Experimental data obtained from Dalgaard and Larsen (42). **b** 60 min after systemic administration. Experimental data obtained from Lund-Anderson *et al.* (44) **c** 63 min after systemic administration. Experimental data obtained from Larsen *et al.* (43).

parameters, for the fluorescein and FG combination, obtained through the regression analysis were as follows:

- $\gamma = (2.0 \pm 0.6) \times 10^{-5} \text{ s}^{-1}$
- $k_{sc} = (2.0 \pm 0.35) \times 10^{-5} \text{ cm/s}$
- $k_{act} = 8.54 \times 10^{-6} \text{ cm/s}$

Using the best fit parameter values based on Palestine and Brubaker's data, we simulated other experiments (42–44). Fig. 4 shows concentration distribution within the retina as reported by Dalgaard and Larsen (42) (Fig. 4a), Lund-Anderson *et al.* (44) (Fig. 4b), and Larsen *et al.* (43) (Fig. 4c), with the model input being the blood fluorescein concentration as reported by the experimenters. The simulations show good qualitative agreement with Dalgaard, except that it over predicts the fluorescein concentration near the retina. Likewise, the simulation predicts fluorescein levels similar to those reported by Lund-Anderson (Fig. 4b) but shows a steeper profile near the retina. The simulation under predicted the fluorescein level when compared to Larsen (Fig. 4c). Given that no fitting parameters were used and individual variations were likely to affect the experimental results as differences in anatomy and/or physiology could have significant effects on the profile, the performance of the model was deemed acceptable.

References shown in Table III report the ratio of outward permeability to inward permeability. Outward permeability in the experiments represents the strength of active transport and the inward permeability represents the strength of passive transport. The first six references in Table III, and the experimental data of Figs. 3 and 4 do not distinguish

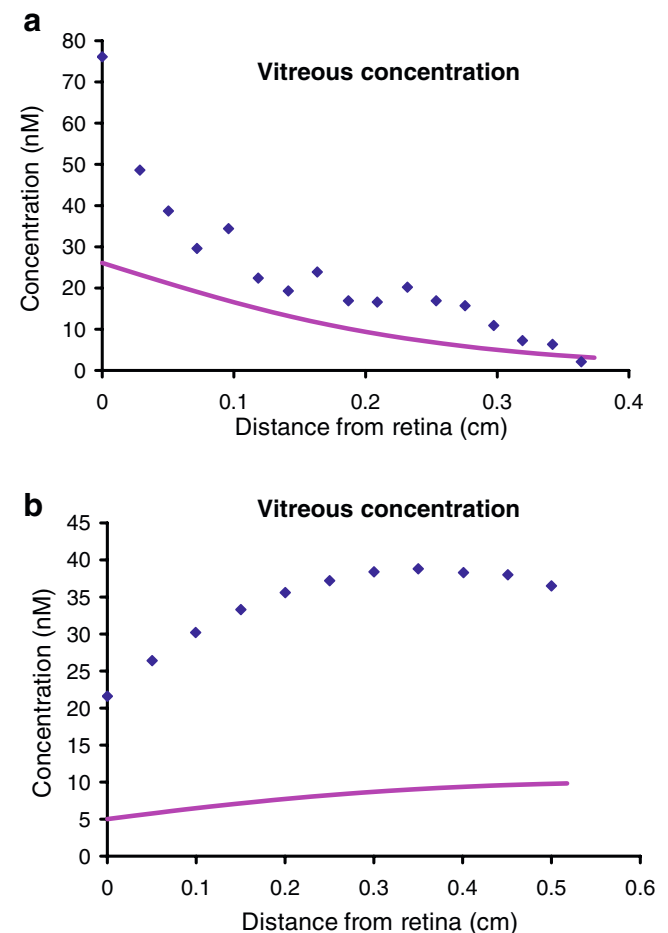


Fig. 5. Comparison of simulated and experimental vitreous fluorescein concentrations based on experimental data by Engler *et al.* (28) **(a)** 1 h after systemic administration. **(b)** 7 h after systemic administration (only the trend-line for the experimental data points are shown).

between fluorescein and FG. The distinction is important because it has been shown (16,28,37,38) that there is a significant difference between the strength of active transport for fluorescein and FG. Yoshida *et al.* (16) performed tests on monkey eyes and found that the ratio of strength of unidirectional to bidirectional transport (Pe^*) between the vitreous and blood for fluorescein was five times as large as

that for FG (see Table III). Engler *et al.* (28) used a differential spectrofluorometry method that separated the contribution of FG to the total fluorescence in the vitreous and the plasma. Their study on human volunteers showed that Pe^* for fluorescein alone was 109. Yoshida *et al.* also found that the difference in the passive permeability of fluorescein and FG is relatively small. Hence, the bidirec-

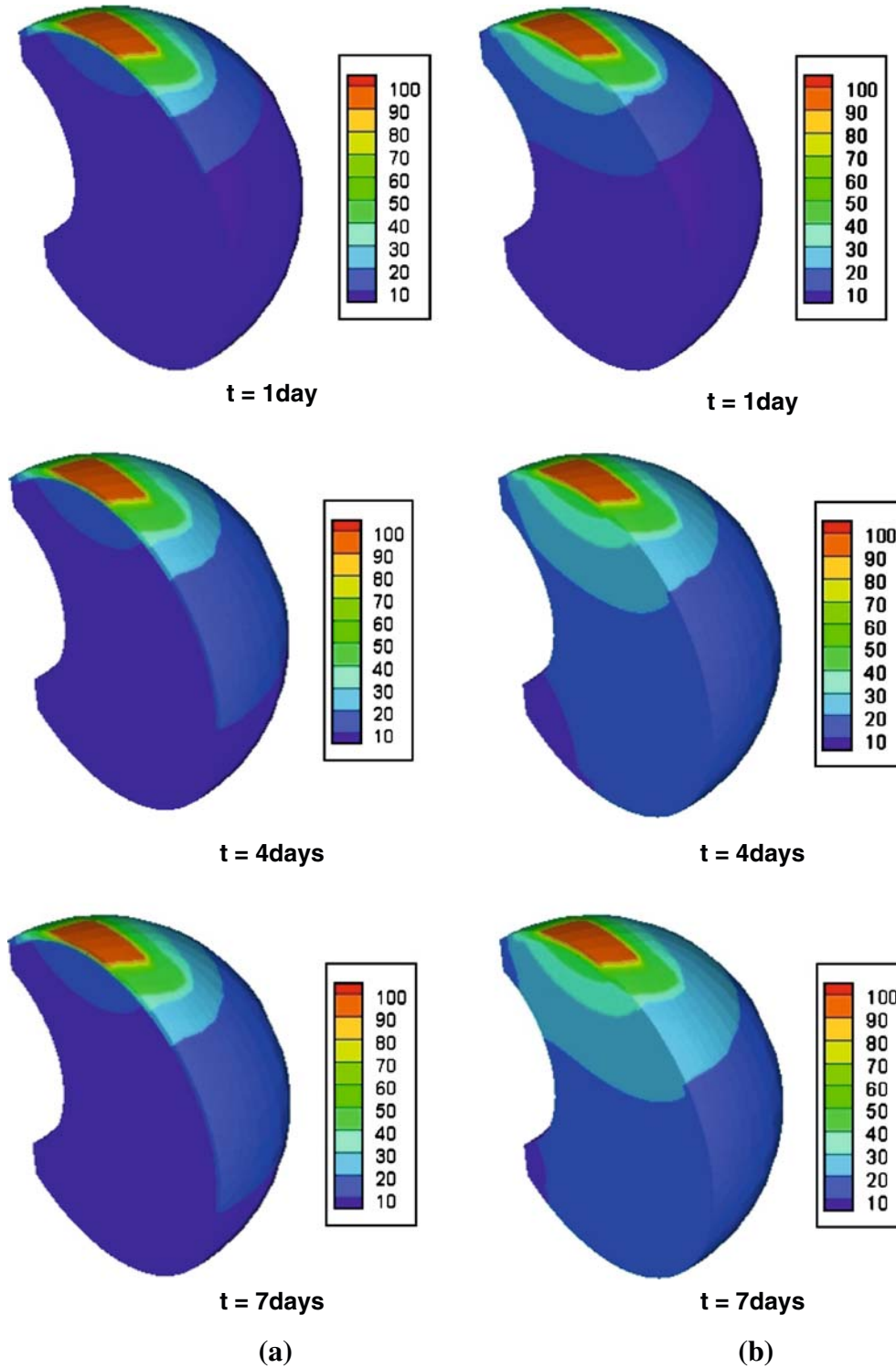


Fig. 6. Concentration profiles with (a) and without (b) active transport in the retina at times $t=1, 4,$ and 7 days after transscleral drug administration.

tional component in Eq. 10 was assumed to be the same for fluorescein and FG. Pe^* was set to 109 and k_{act} , for the active transport of fluorescein alone, was recalculated to be 3.1×10^{-5} cm/s. Fig. 5a and b shows the comparison between the experimental results obtained by Engler *et al.* (28) for the movement of fluorescein alone in the vitreous and the model results with the revised k_{act} value. The deviation of the simulation result from the experimental result seen in Fig. 5b could indicate an overestimation of k_{act} , which would lead to higher clearance of the drug once the systemic levels started to drop. The disagreement could also be due to the difference in the passive permeability values of fluorescein and FG. Possible explanations for the deviation are presented in “Discussion” of the paper.

The computer model with the evaluated parameters was also used to simulate transscleral drug delivery. A drug source with constant concentration was assumed on the surface of the sclera. The simulations were run with and without the active transport term for the RPE and the results for the two cases are depicted in Fig. 6a and b. Significant periscleral movement of the drug in the presence of active transport was observed from the simulations. Such a phenomenon has not been reported in experimental literature based on transscleral delivery, but there has been very little examination of the sclera at long periods after drug administration. Vollmer *et al.* (45) evaluated the distribution of the aminoglycoside antibiotic amikacin in the ocular tissues in rabbit eyes following transscleral iontophoresis for 20 min. Their results for the case with zero iontophoretic current show that the concentration of the drug in the non-treated hemisphere of the sclera is insignificant when compared to the treated hemisphere of the sclera. The measurements were, however, taken 30 min following iontophoresis and significant periscleral transport could not be observed at such short periods. Given the complexities of electrolyte transport, simulating iontophoresis would require a significant alteration of the current model.

DISCUSSION

Transscleral delivery has been identified as a potentially effective drug delivery system to treat posterior segment eye diseases. The drug source is placed in the periorbital space, whence the drug can permeate to the target tissue through the anterior chamber, *via* the systemic circulation, or through the direct penetration pathway. The relative contributions of these routes have been investigated in rabbits and rats (46–48), and the direct penetration route was found to be the most important in terms of drug concentrations attained in the vitreous. The direct penetration pathway however, involves several tissue related barriers and elimination factors. These factors include clearance *via* episcleral veins and conjunctival blood and lymphatic flow, diffusion across the sclera, clearance *via* choroidal circulation, diffusion across the Bruch’s membrane, RPE and the retina, and active transport in RPE.

Passive diffusion across the sclera has been studied extensively (5–10), and the sclera has been shown to be permeable to a wide molecular weight range of solutes. Similar studies (14,15,49–51) have also been conducted on isolated RPE and Bruch’s membrane to estimate the passive *in vitro* permeability of the excised tissues to various molecules. However, there is no quantitative information available on the effect of the active

barriers and clearance factors, some of which could be significant, on the movement of the drug molecules *via* the direct penetration pathway. Our model quantitates these factors and evaluates their effect on the movement of the drug molecules *via* the direct penetration pathway.

Based on the parameter values for fluorescein we evaluate three key dimensionless numbers

1. The square of the Thiele modulus: $\Phi^2 = \gamma L_{cs}^2 / D_{cs} = 0.032$
2. Péclet number for active transport: $Pe = (k_{act} + v_{ret}) L_{rpe} / D_{rpe} = 1.2$
3. Biot number for mass transfer at the scleral surface: $Bi = k_{sc} L_{cs} / D_{cs} = 0.81$

where v_{ret} is the average velocity of aqueous permeation at the retinal surface. The dimensionless numbers are used to assess the significance of the active barriers and clearance factors affecting transscleral drug movement.

Choroidal circulation has been suspected to have a significant effect on drug transport in the posterior eye. The choroidal blood flow is high for its weight, and the choriocapillaris walls contain large fenestrations (52) suggesting that the choroidal flow could act as a sink for molecules diffusing across it. However, there is very little information on the effect of choroidal clearance on transscleral delivery. Bill (53) and Törnquist (54) both found that large macromolecules were able to enter the blood vessels through the fenestrations. Kim *et al.* (36) used episcleral implants on rabbits and observed negligible vitreous concentrations during *in vivo* experiments but significant vitreous concentrations in their *ex vivo* experiments. They had attributed the observed difference to the choroidal blood flow and hence, had assumed the choroid to be a complete sink in their computational model. The Thiele modulus, calculated in the previous paragraph suggests that most of the drug molecules diffuse through the choroid without being washed away by the blood flow and hence, clearance by the blood flow is not as important a factor as previously thought. The study by Robinson *et al.* (18) supports this finding. Robinson *et al.* had developed a rabbit model to study the effects of choroidal clearance on the transscleral delivery of triamcinolone acetonide. The study involved using cryotherapy to eliminate the choroidal blood flow in the area close to the drug source. The results of the study showed that elimination of the conjunctival lymphatic/blood vessels was more effective in increasing vitreal concentrations than the elimination of the choroidal vessels. Raviola (55) also observed that the conjunctival and episcleral blood vessels are highly permeable to blood-borne horseradish peroxidase. The Biot number calculated in the previous section shows that clearance of the drug from the scleral surface is comparable to the diffusion of the drug through the sclera, which is in agreement with the observation made by Robinson *et al.*

The evaluation of the importance of active transport mechanism in the RPE, as one of the barriers to delivering drugs through the transscleral route, was the second goal of the study. Active pumping of fluorescein from the vitreous to the blood was first observed by Cunha-Vaz and Maurice (13). Since then, a number of investigators (23–25,27) have calculated the resistance to the movement of fluorescein and FG from the vitreous to the blood and vice versa. These

studies, however, did not differentiate between transport across the RPE layer and diffusion through the walls of the blood vessels. Our model separates the two, and hence we are able to determine the effect of these barriers separately. The Péclet number for active transport suggests that the diffusion of fluorescein through the RPE layer is equally opposed by the active transport mechanism. This balance could be critical for high molecular weight, hydrophilic drugs, which permeate poorly the tight junctions between the pigment epithelium cells (56). Thus the rate-limiting barrier for transscleral delivery could potentially be the retina and its pigment epithelium. The importance of active transport on the posterior eye concentrations attained after transscleral delivery can be gauged from Fig. 6a and b. Including active transport in the simulations resulted in significant periscleral transport, which tended to produce more rapid distribution (Fig. 6, 1 day) and elevated drug concentration around the sclera. Although such a result has not been reported in the experimental literature, it presents an excellent opportunity to assess the role of active RPE transport in future experiments by examining drug distribution around the sclera. It should be noted, though, that a very simplistic approach has been used to model active transport, which is compound specific and non-linear in other tissues of the body. Nevertheless, the linear model could be used as a semi-quantitative tool to assess the strength of the active transport mechanism. Also, the fit discussed earlier was repeated without active transport and the root mean square error in the fit of Fig. 3a increased from 2.3×10^{-3} to 2.7×10^{-3} , a change of 20%, and the value of k_{sc} increased from 2.0×10^{-5} to 3.1×10^{-5} cm/s, with the increase obviously needed to make up for the lack of active transport. Thus, it is recognized that the ability to fit the data of Fig. 3a is not *per se* a good test of how important active transport effects are. With the advent of detailed bio-analytical methods, it may be possible in the future to evaluate better the contribution of active transport.

The simulation results for fluorescein were based on the assumption that the difference in passive, bidirectional transport of fluorescein and FG between the blood and the vitreous was relatively small. The assumption was based on the observation by Yoshida *et al.* (16) that the ratio of inward permeability (blood to vitreous) of FG to fluorescein to be 1.3 ± 0.3 . The result was surprising as the passive permeation of fluorescein is expected to be higher than FG, since fluorescein has lower molecular weight and higher lipid solubility than FG. A detailed explanation on the possible reasons for this result is provided in Lund-Anderson *et al.* (57) and Yoshida *et al.* (16). Our evaluation of k_{act} would be an overestimate if the permeability of fluorescein through the barrier was indeed higher, which would explain the deviation of the simulation result from the experimental result shown in Fig. 5a and b. A lower k_{act} would result in higher vitreous concentrations and would reduce the error between the simulation and experimental results shown in the figure. The error is less in the 1 h case (Fig. 5a) when compared to the 7 h case (Fig. 5b) because the effect of k_{act} is felt less immediately after systemic injection and it increases as the vitreous concentrations increase. More detailed experimental evaluation of the permeability of fluorescein and FG through the blood-vitreous barrier is needed to get a better estimate of k_{act} from the model, and a more detailed view of transport in

the retina, choroid, and sclera [e.g., (58)] may also be necessary.

In summary, we have developed a computational model of transport in the posterior eye that takes into account loss of drug to the choroidal circulation, active transport by the retinal pigment epithelium layer and the clearance by the conjunctival lymphatics and blood flow in the episcleral veins. These factors are critical in transscleral drug administration and in predicting posterior eye concentrations, as they are potential barriers to the movement of drug molecule into the posterior eye. The model, however, deals only with fluorescein, and care should be taken when extrapolating the results to other drugs, which could have different physical and chemical properties. The results of the study show that losses to choroidal circulation are not as important an impeding factor as thought previously. In contrast, the mass transfer from the scleral surface was found to be significant and hence, design of the drug source to be placed on the scleral surface needs more attention. Pontes de Carvalho *et al.* (59) showed that sealing an impermeable drug source to the sclera results in selective diffusion through the sclera and minimizes loss to the episcleral space. Active transport by the RPE has not been considered completely in any of the computational models developed thus far, and our results show that it could play an important role, not only in impeding the transscleral movement of drug molecules but also in affecting the transport pathway of the drug molecules.

ACKNOWLEDGEMENTS

This work was supported by the Institute for Engineering and Medicine (IEM) at the University of Minnesota and by the National Institutes of Health (R03-EB007815). The resources provided by the Minnesota Supercomputing Institute (MSI) at the University of Minnesota were used for running the simulations. We thank Phil Bransford, who helped us in the initial stages of model building and Matt Stay for providing valuable insights on the subject matter.

APPENDIX

Sensitivity Computation for Gauss-Newton Scheme

Squared curve-fitting problem amounts to minimizing the error between the simulations and experimental results,

$$E = \left(c_{\text{exp}} - \frac{1}{V} \int_v c \, dv \right)^2 \quad (11)$$

where c_{exp} is the average concentration observed experimentally. The Gauss-Newton scheme finds the minimum iteratively, requiring partial derivatives of the objective function E , with respect to the parameters, e.g.,

$$\frac{\partial}{\partial \gamma} \left(c_{\text{exp}} - \frac{1}{V} \int_v c \, dv \right)^2 = -2 \left(c_{\text{exp}} - \frac{1}{V} \int_v c \, dv \right) \left(\frac{1}{V} \int_v \frac{\partial c}{\partial \gamma} \, dv \right) \quad (12)$$

The sensitivities s_γ and $s_{k_{sc}}$ are defined as

$$s_\gamma \equiv \frac{\partial c}{\partial \gamma} \text{ and } s_{k_{sc}} \equiv \frac{\partial c}{\partial k_{sc}} \quad (13)$$

The mass balance Eqs. 3, 4 and 5 along with boundary conditions 7, 8 and 9 are differentiated with respect to γ and k_{sc} to obtain the following relationships which would be solved for s_γ and $s_{k_{sc}}$ respectively.

Equations and Boundary Conditions for s_γ

1. Domain equations

$$\text{Vitreous} : \frac{\partial s_\gamma}{\partial t} + v \cdot \nabla s_\gamma - D_v \nabla^2 s_\gamma = 0 \quad (14)$$

$$\text{RPE} : \frac{\partial s_\gamma}{\partial t} + (v + k_{act}) \cdot \nabla s_\gamma - D_{rpe} \nabla^2 s_\gamma = -\frac{\partial k_{act}}{\partial \gamma} \cdot \nabla c \quad (15)$$

$$\text{CS} : \frac{\partial s_\gamma}{\partial t} + v \cdot \nabla s_\gamma - D_{cs} \nabla^2 s_\gamma + \gamma s_\gamma = (c_{bl} - c) \quad (16)$$

2. Boundary conditions

$$\text{Lens} : n \cdot (-D \nabla s_\gamma + v s_\gamma) = 0 \quad (17)$$

$$\text{Hyaloid} : n \cdot (-D \nabla s_\gamma + v s_\gamma) = k_{hy} s_\gamma \quad (18)$$

$$\text{Sclera} : n \cdot (-D \nabla s_\gamma + v s_\gamma) = k_{sc} s_\gamma \quad (19)$$

where $\left\| \frac{\partial k_{act}}{\partial \gamma} \right\| = \frac{Pe^* L_{rpe}}{\left(\frac{L_{rpe}^2}{D_{rpe}} + \frac{L_{cs}^2}{D_{cs}} + \frac{1}{\gamma} \right)^2} \left(\frac{1}{\gamma^2} \right)$ from Eq. 10, and the vector points in the same direction as k_{act} .

Equations and Boundary Conditions for $s_{k_{sc}}$

1. Domain equations

$$\text{Vitreous} : \frac{\partial s_{k_{sc}}}{\partial t} + v \cdot \nabla s_{k_{sc}} - D_v \nabla^2 s_{k_{sc}} = 0 \quad (20)$$

$$\text{RPE} : \frac{\partial s_{k_{sc}}}{\partial t} + (v + k_{act}) \cdot \nabla s_{k_{sc}} - D_{rpe} \nabla^2 s_{k_{sc}} = 0 \quad (21)$$

$$\text{CS} : \frac{\partial s_{k_{sc}}}{\partial t} + v \cdot \nabla s_{k_{sc}} - D_{cs} \nabla^2 s_{k_{sc}} + \gamma s_{k_{sc}} = 0 \quad (22)$$

2. Boundary conditions

$$\text{Lens} : n \cdot (-D \nabla s_{k_{sc}} + v s_{k_{sc}}) = 0 \quad (23)$$

$$\text{Hyaloid} : n \cdot (-D \nabla s_{k_{sc}} + v s_{k_{sc}}) = k_{hy} s_{k_{sc}} \quad (24)$$

$$\text{Sclera} : n \cdot (-D \nabla s_{k_{sc}} + v s_{k_{sc}}) = k_{sc} s_{k_{sc}} + c \quad (25)$$

The average values of s_γ and $s_{k_{sc}}$ over the vitreous volume were calculated and used for the Gauss–Newton curve fitting algorithm.

REFERENCES

1. T. Yasukawa, Y. Ogura, Y. Tabata, H. Kimura, P. Wiedemann, and Y. Honda. Drug delivery systems for vitreoretinal diseases. *Prog. Retin. Eye Res.* **23**:253–281 (2004). doi:10.1016/j.preteyeres.2004.02.003.
2. G. M. Bleeker, N. J. van Haeringen, E. R. Maas, and E. Glasius. Selective properties of the vitreous barrier. *Exp. Eye Res.* **7**:37–46 (1968). doi:10.1016/S0014-4835(68)80024-7.
3. P. M. Hughes, O. Olejnik, J. E. Chang-Lin, and C. G. Wilson. Topical and systemic drug delivery to the posterior segments. *Adv. Drug Deliv. Rev.* **57**:2010–2032 (2005). doi:10.1016/j.addr.2005.09.004.
4. D. H. Geroski, and H. F. Edelhauser. Drug delivery for posterior segment eye disease. *Invest. Ophthalmol. Vis. Sci.* **41**:961–964 (2000).
5. I. Ahmed, and T. F. Patton. Importance of the noncorneal absorption route in topical ophthalmic drug delivery. *Invest. Ophthalmol. Vis. Sci.* **26**:584–587 (1985).
6. J. Ambati, E. S. Gragoudas, J. W. Miller, T. T. You, K. Miyamoto, F. C. Delori, and A. P. Adamis. Transscleral delivery of bioactive protein to the choroid and retina. *Invest. Ophthalmol. Vis. Sci.* **41**:1186–1191 (2000).
7. J. Ambati, C. S. Canakis, J. W. Miller, E. S. Gragoudas, A. Edwards, D. J. Weissgold, I. Kim, F. C. Delori, and A. P. Adamis. Diffusion of high molecular weight compounds through sclera. *Invest. Ophthalmol. Vis. Sci.* **41**:1181–1185 (2000).
8. A. Bill. Movement of albumin and dextran through the sclera. *Arch. Ophthalmol.* **74**:248–252 (1965).
9. D. M. Maurice, and J. Polgar. Diffusion across the sclera. *Exp. Eye Res.* **25**:577–582 (1977). doi:10.1016/0014-4835(77)90136-1.
10. T. W. Olsen, H. F. Edelhauser, J. I. Lim, and D. H. Geroski. Human scleral permeability. Effects of age, cryotherapy, transscleral diode laser, and surgical thinning. *Invest. Ophthalmol. Vis. Sci.* **36**:1893–1903 (1995).
11. S. C. Pflugfelder, E. Hernandez, S. J. Fliesler, J. Alvarez, M. E. Pflugfelder, and R. K. Forster. Intravitreal vancomycin. Retinal toxicity, clearance, and interaction with gentamicin. *Arch. Ophthalmol.* **105**:831–837 (1987).
12. S. Tsuboi. Measurement of the volume flow and hydraulic conductivity across the isolated dog retinal pigment epithelium. *Invest. Ophthalmol. Vis. Sci.* **28**:1776–1782 (1987).
13. J. G. Cunha-Vaz, and D. M. Maurice. The active transport of fluorescein by the retinal vessels and the retina. *J. Physiol.* **191**:467–486 (1967).
14. M. Kimura, M. Araie, and S. Koyano. Movement of carboxy-fluorescein across retinal pigment epithelium-choroid. *Exp. Eye Res.* **63**:51–56 (1996). doi:10.1006/exer.1996.0090.
15. S. Koyano, M. Araie, and S. Eguchi. Movement of fluorescein and its glucuronide across retinal pigment epithelium-choroid. *Invest. Ophthalmol. Vis. Sci.* **34**:531–538 (1993).
16. A. Yoshida, S. Ishiko, and M. Kojima. Outward permeability of the blood-retinal barrier. *Graefes Arch. Clin. Exp. Ophthalmol.* **230**:78–83 (1992). doi:10.1007/BF00166767.
17. M. S. Stay, J. Xu, T. W. Randolph, and V. H. Barocas. Computer simulation of convective and diffusive transport of controlled-

- release drugs in the vitreous humor. *Pharm. Res.* **20**:96–102 (2003). doi:10.1023/A:1022207026982.
18. M. R. Robinson, S. S. Lee, H. Kim, S. Kim, R. J. Lutz, C. Galban, P. M. Bungay, P. Yuan, N. S. Wang, J. Kim, and K. G. Csaky. A rabbit model for assessing the ocular barriers to the transscleral delivery of triamcinolone acetonide. *Exp. Eye Res.* **82**:479–487 (2006). doi:10.1016/j.exer.2005.08.007.
 19. I. A. Sigal, J. G. Flanagan, and C. R. Ethier. Factors influencing optic nerve head biomechanics. *Invest. Ophthalmol. Vis. Sci.* **46**:4189–4199 (2005). doi:10.1167/iovs.05-0541.
 20. I. Fatt, and B. O. Hedbys. Flow of water in the sclera. *Exp Eye Res.* **10**:243–249 (1970). doi:10.1016/S0014-4835(70)80035-5.
 21. J. Xu, J. J. Heys, V. H. Barocas, and T. W. Randolph. Permeability and diffusion in vitreous humor: implications for drug delivery. *Pharm. Res.* **17**:664–669 (2000). doi:10.1023/A:1007517912927.
 22. V. P. Ranta, and A. Urtti. Transscleral drug delivery to the posterior eye: prospects of pharmacokinetic modeling. *Adv. Drug Deliv. Rev.* **58**:1164–1181 (2006). doi:10.1016/j.addr.2006.07.025.
 23. N. P. Blair, R. C. Zeimer, M. M. Rusin, and J. G. Cunha-Vaz. Outward transport of fluorescein from the vitreous in normal human subjects. *Arch. Ophthalmol.* **101**:1117–1121 (1983).
 24. K. Miyake. Outward transport of fluorescein from vitreous in eyes with intraocular surgeries. *Jpn. J. Ophthalmol.* **38**:1091–1096 (1984).
 25. Y. Oguro, Y. Tsukahara, I. Saito, and T. Kondo. Estimation of the permeability of the blood-retinal barrier in normal individuals. *Invest. Ophthalmol. Vis. Sci.* **26**:969–976 (1985).
 26. A. G. Palestine, and R. F. Brubaker. Pharmacokinetics of fluorescein in the vitreous. *Invest. Ophthalmol. Vis. Sci.* **21**:542–549 (1981).
 27. R. C. Zeimer, N. P. Blair, and J. G. Cunha-Vaz. Pharmacokinetic interpretation of vitreous fluorophotometry. *Invest. Ophthalmol. Vis. Sci.* **24**:1374–1381 (1983).
 28. C. B. Engler, B. Sander, M. Larsen, P. Dalgaard, and H. Lund-Andersen. Fluorescein transport across the human blood-retina barrier in the direction vitreous to blood. Quantitative assessment *in vivo*. *Acta Ophthalmol. (Copenh)*. **72**:655–662 (1994).
 29. C. R. Ethier, M. Johnson, and J. Ruberti. Ocular biomechanics and biotransport. *Annu. Rev. Biomed. Eng.* **6**:249–273 (2004). doi:10.1146/annurev.bioeng.6.040803.140055.
 30. R. D. Schoenwald, G. S. Deshpande, D. G. Rethwisch, and C. F. Barfknecht. Penetration into the anterior chamber *via* the conjunctival/scleral pathway. *J. Ocular Pharmacol. Ther.* **13**:41–59 (1997).
 31. R. J. Kaiser, and D. M. Maurice. The diffusion of fluorescein in the lens. *Exp. Eye Res.* **3**:156–165 (1964). doi:10.1016/S0014-4835(64)80030-0.
 32. D. M. Maurice. Drug delivery to the posterior segment from drops. *Surv. Ophthalmol.* **47**(Suppl 1):S41–S52 (2002). doi:10.1016/S0039-6257(02)00326-0.
 33. P. Blondeau, J. P. Tetrault, and C. Papamarkakis. Diurnal variation of episcleral venous pressure in healthy patients: a pilot study. *J. Glaucoma.* **10**:18–24 (2001). doi:10.1097/00061198-200102000-00005.
 34. P. J. Missel. Hydraulic Flow and Vascular Clearance Influences on Intravitreal Drug Delivery. *Pharm. Res.* **19**:1636–1647 (2002). doi:10.1023/A:1020940927675.
 35. H. Kim, M. J. Lizak, G. Tansey, K. G. Csaky, M. R. Robinson, P. Yuan, N. S. Wang, and R. J. Lutz. Study of ocular transport of drugs released from an intravitreal implant using magnetic resonance imaging. *Ann. Biomed. Eng.* **33**:150–164 (2005). doi:10.1007/s10439-005-8974-7.
 36. H. Kim, M. R. Robinson, M. J. Lizak, G. Tansey, R. J. Lutz, P. Yuan, N. S. Wang, and K. G. Csaky. Controlled drug release from an ocular implant: an evaluation using dynamic three-dimensional magnetic resonance imaging. *Invest. Ophthalmol. Vis. Sci.* **45**:2722–2731 (2004). doi:10.1167/iovs.04-0091.
 37. N. P. Blair, M. A. Evans, T. S. Lesar, and R. C. Zeimer. Fluorescein and fluorescein glucuronide pharmacokinetics after intravenous injection. *Invest. Ophthalmol. Vis. Sci.* **27**:1107–1114 (1986).
 38. S. Kitano, and S. Nagataki. Transport of fluorescein monoglucuronide out of the vitreous. *Invest. Ophthalmol. Vis. Sci.* **27**:998–1001 (1986).
 39. P. R. Amestoy, and J. Y. L'Excellent. MUMPS Multifrontal massively parallel solver, version 2.0. *J. Phys. Condens. Matter.* **10**:7975 (1998). doi:10.1088/0953-8984/10/36/008.
 40. M. Araie, and D. M. Maurice. The loss of fluorescein, fluorescein glucuronide and fluorescein isothiocyanate dextran from the vitreous by the anterior and retinal pathways. *Exp. Eye Res.* **52**:27–39 (1991). doi:10.1016/0014-4835(91)90125-X.
 41. J. Park, P. M. Bungay, R. J. Lutz, J. J. Augsburger, R. W. Millard, A. Sinha Roy, and R. K. Banerjee. Evaluation of coupled convective-diffusive transport of drugs administered by intravitreal injection and controlled release implant. *J. Control Release.* **105**:279–295 (2005). doi:10.1016/j.jconrel.2005.03.010.
 42. P. Dalgaard, and M. Larsen. Fitting numerical solutions of differential equations to experimental data: a case study and some general remarks. *Biometrics.* **46**:1097–1109 (1990). doi:10.2307/2532451.
 43. J. Larsen, H. Lund-Andersen, and B. Krogsaa. Transient transport across the blood-retina barrier. *Bull. Math. Biol.* **45**:749–758 (1983).
 44. H. Lund-Andersen, B. Krogsaa, M. la Cour, and J. Larsen. Quantitative vitreous fluorophotometry applying a mathematical model of the eye. *Invest. Ophthalmol. Vis. Sci.* **26**:698–710 (1985).
 45. D. L. Vollmer, M. A. Szlek, K. Kolb, L. B. Lloyd, and T. M. Parkinson. *In vivo* transscleral iontophoresis of amikacin to rabbit eyes. *J. Ocul. Pharmacol. Ther.* **18**:549–558 (2002). doi:10.1089/108076802321021090.
 46. S. P. Ayalasomayajula, and U. B. Kompella. Retinal delivery of celecoxib is several-fold higher following subconjunctival administration compared to systemic administration. *Pharm. Res.* **21**:1797–1804 (2004). doi:10.1023/B:PHAM.0000045231.51924.e8.
 47. T. W. Lee, and J. R. Robinson. Drug delivery to the posterior segment of the eye: some insights on the penetration pathways after subconjunctival injection. *J. Ocular Pharmacol Ther.* **17**:565–572 (2001). doi:10.1089/10807680152729257.
 48. A. Tsuji, I. Tamai, and K. Sasaki. Intraocular penetration kinetics of prednisolone after subconjunctival injection in rabbits. *Ophthalmic Res.* **20**:31–43 (1988).
 49. N. P. Cheruvu, and U. B. Kompella. Bovine and porcine transscleral solute transport: influence of lipophilicity and the Choroid–Bruch's layer. *Invest. Ophthalmol. Vis. Sci.* **47**:4513–4522 (2006). doi:10.1167/iovs.06-0404.
 50. S. Tsuboi, and J. E. Pederson. Permeability of the isolated dog retinal pigment epithelium to carboxyfluorescein. *Invest. Ophthalmol. Vis. Sci.* **27**:1767–1770 (1986).
 51. S. Tsuboi, T. Fujimoto, Y. Uchihori, K. Emi, S. Iizuka, K. Kishida, and R. Manabe. Measurement of retinal permeability to sodium fluorescein *in vitro*. *Invest. Ophthalmol. Vis. Sci.* **25**:1146–1150 (1984).
 52. A. Bill, P. Tornquist, and A. Alm. Permeability of the intraocular blood vessels. *Trans. Ophthalmol. Soc. U. K.* **100**:332–336 (1980).
 53. A. Bill. Capillary permeability to and extravascular dynamics of myoglobin, albumin and gammaglobulin in the uvea. *Acta Physiol. Scand.* **73**:204–219 (1968).
 54. P. Tornquist. Capillary permeability in cat choroid, studied with the single injection technique (II). *Acta Physiol. Scand.* **106**:425–430 (1979).
 55. G. Raviola. Conjunctival and episcleral blood vessels are permeable to blood-borne horseradish peroxidase. *Invest. Ophthalmol. Vis. Sci.* **24**:725–736 (1983).
 56. L. Pitkanen, V. P. Ranta, H. Moilanen, and A. Urtti. Permeability of retinal pigment epithelium: effects of permeant molecular weight and lipophilicity. *Invest. Ophthalmol. Vis. Sci.* **46**:641–646 (2005)doi:10.1167/iovs.04-1051.
 57. H. Lund-Andersen, M. Larsen, P. Dalgaard, and W. Olsen. Fluorescein and fluorescein glucuronide in the vitreous body of diabetic patients. *Graefes. Arch. Clin. Exp. Ophthalmol.* **225**:173–176 (1987). doi:10.1007/BF02175445.
 58. F. Mac Gabhann, A. Demetriades, T. Deering, J. Packer, S. Shah, E. Duh, P. Campochiaro, and A. Popel. Protein transport to choroid and retina following periorcular injection: theoretical and experimental study. *Ann. Biomed. Eng.* **35**:615–630 (2007).
 59. R. A. Pontes de Carvalho, M. L. Krausse, A. L. Murphree, E. E. Schmitt, P. A. Campochiaro, and I. H. Maumenee. Delivery from episcleral explants. *Invest. Ophthalmol. Vis. Sci.* **47**:4532–4539 (2006). doi:10.1167/iovs.06-0030.

60. A. Ohtori, and K. Tojo. *In vivo/in vitro* correlation of intravitreal delivery of drugs with the help of computer simulation. *Biol. Pharm. Bull.* **17**:283–290 (1994).
61. S. Friedrich, Y. L. Cheng, and B. Saville. Drug distribution in the vitreous humor of the human eye: the effects of intravitreal injection position and volume. *Curr. Eye Res.* **16**:663–669 (1997). doi:10.1076/ceyr.16.7.663.5061.
62. S. Friedrich, B. Saville, and Y. L. Cheng. Drug distribution in the vitreous humor of the human eye: the effects of aphakia and changes in retinal permeability and vitreous diffusivity. *J. Ocular Pharmacol. Ther.* **13**:445–459 (1997).
63. S. Friedrich, Y. L. Cheng, and B. Saville. Finite element modeling of drug distribution in the vitreous humor of the rabbit eye. *Ann. Biomed. Eng.* **25**:303–314 (1997). doi:10.1007/BF02648045.